Caffeic Acid Grafted PLGA as a Novel Material for the Design of Fluvastatin Eluting Nanoparticles for the Prevention of Neointimal Hyperplasia

Journal:	*Molecular Pharmaceutics*
Manuscript ID	mp-2022-00693j.R1
Manuscript Type:	Article
Date Submitted by the Author:	n/a
Complete List of Authors:	Bellosta, Stefano; Universita degli Studi di Milano, Department of Pharmacological and Biomolecular Sciences Selmin, Francesca; Università degli Studi di Milano, Department of Pharmaceutical Sciences Magri, Giulia; Universita degli Studi di Milano, Department of Pharmaceutical Sciences Castiglioni, Silvia; Università degli Studi di Milano, Department of Pharmacological and Biomolecular Sciences Procacci, Patrizia; Universita degli Studi di Milano, Biomedical Sciences for Health Sartori, Patrizia; Università degli Studi di Milano, Department of Biomedical Sciences for Health Scarpa, Edoardo; Universita degli Studi di Milano, Department of Pharmaceutical Sciences; National Molecular Genetics Institute Foundation Tolva, Valerio; ASST Grande Ospedale Metropolitano Niguarda, Struttura Complessa di Chirurgia Vascolare. Fondazione "A. De Gasperis" Rossi, Clara; Università degli Studi di Milano, Department of Pharmacological and Biomolecular Sciences Puoci, Francesco; University of Calabria, Department of Pharmacy Rizzello, Loris; University of Milan, Department of Pharmaceutical Sciences; National Molecular Genetics Institute Foundation Cilurzo, Francesco; Universita degli Studi di Milano, Department of Pharmaceutical Sciences

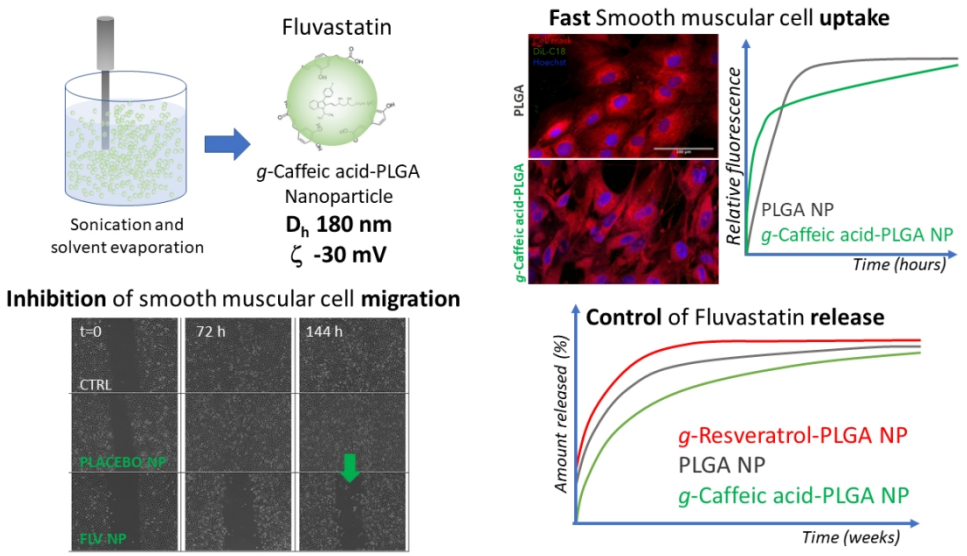

Drug eluting nanoparticles (NP) administered by eluting balloon represent a novel tool to prevent restenosis after angioplasty, even if the selection of the suitable drug and biodegradable material is still matter of debate. Herein, we provide the proof of concept of the use of a novel material obtained by combining the grafting of caffeic acid or resveratrol on a poly(lactide-co-glycolide) backbone (g-CA-PLGA or g-RV-PLGA) and the pleiotropic effects of fluvastatin chosen because of its low lipophilic profile which is challenging for the encapsulation in nanoparticles and delivery to the artery wall cells. NP made of such materials are biocompatible with macrophages, human smooth muscle cells (SMC) and endothelial cells (EC). Their cellular uptake is demonstrated and quantified by confocal microscopy using fluorescent NP; while their distribution in cytoplasm is verified by TEM images, using NP stained with an Ag-PVP probe appositely synthetized. g-CA-PLGA assures the best control of the FLV release from NP sizing around 180 nm and the faster SMC uptake, as demonstrated by confocal analyses. Interestingly and surprisingly, g-CA-PLGA improves the FLV efficacy to inhibit the SMC migration, without altering its effects on EC proliferation and migration. The improved trophism on nanoparticles towards SMC combined with the excellent biocompatibility and low modification of microenvironment pH upon polymer degradation makes g-CA-PLGA a suitable material for the design of drug eluting balloons

338x190mm (96 x 96 DPI)

Caffeic Acid Grafted PLGA as a Novel Material for the Design of Fluvastatin Eluting Nanoparticles for the Prevention of Neointimal Hyperplasia

Stefano Bellosta[1§], Francesca Selmin[2§], Giulia Magri[2†], Silvia Castiglioni[1], Patrizia Procacci[3], Patrizia Sartori[3], Edoardo Scarpa[2,4], Valerio Tolva[5], Clara Rossi[1], Francesco Puoci[6], Loris Rizzello[2,4], Francesco Cilurzo[2]*

[1] Dept. Pharmacological and Biomolecular Sciences, Via G. Balzaretti 9, Università degli Studi di Milan - Milan, Italy

[2] Dept of Pharmaceutical Sciences, Università degli Studi di Milano, via G. Colombo, 71 - Milan, Italy

[3] Dept of Biomedical Sciences for Health, Università degli Studi di Milano - Milan, Italy

[4] National Institute of Molecular Genetics (INGM), Via Francesco Sforza 35 - Milan, Italy

[5] Struttura Complessa di Chirurgia Vascolare. Fondazione "A. De Gasperis". ASST Grande Ospedale Metropolitano Niguarda, Piazza Ospedale Maggiore 3 - Milan, Italy

[6] Dept of Pharmacy, Health and Nutritional Sciences, University of Calabria - Rende, CS, Italy.

[§]The Authors equally contribute to the work

KEYWORDS

Confocal microscopy; DIL; Prolonged release; Silver nanoparticle; fluvastatin; resveratrol.

ABSTRACT

Drug eluting nanoparticles (NP) administered by eluting balloon represent a novel tool to prevent restenosis after angioplasty, even if the selection of the suitable drug and biodegradable material is still matter of debate. Herein, we provide the proof of concept of the use of a novel material obtained by combining the grafting of caffeic acid or resveratrol on a poly(lactide-co-glycolide) backbone (g-CA-PLGA or g-RV-PLGA) and the pleiotropic effects of fluvastatin chosen because of its low lipophilic profile which is challenging for the encapsulation in nanoparticles and delivery

to the artery wall cells. NP made of such materials are biocompatible with macrophages, human smooth muscle cells (SMC) and endothelial cells (EC). Their cellular uptake is demonstrated and quantified by confocal microscopy using fluorescent NP; while their distribution in cytoplasm is verified by TEM images, using NP stained with an Ag-PVP probe appositely synthetized. g-CA-PLGA assures the best control of the FLV release from NP sizing around 180 nm and the faster SMC uptake, as demonstrated by confocal analyses. Interestingly and surprisingly, g-CA-PLGA improves the FLV efficacy to inhibit the SMC migration, without altering its effects on EC proliferation and migration. The improved trophism on nanoparticles towards SMC combined with the excellent biocompatibility and low modification of microenvironment pH upon polymer degradation makes g-CA-PLGA a suitable material for the design of drug eluting balloons.

INTRODUCTION

Cardiovascular diseases are still the primary causes of morbidity and mortality worldwide. Indeed, according to the WHO the ischemic heart disease is responsible for 16% of the world's total deaths. Since year 2000, the largest increase in deaths has been, for this disease, rising by more than 2 million to 8.9 million deaths in 2019. Stroke is the 2nd leading cause of death, being responsible for approximately 11% of total deaths.

Cardiovascular diseases are known to have a complex and multifaceted etiology. A lesioned endothelial layer drives the evolution of the "atheroma" by multiple pathways including: 1) chemotaxis and recruitment of circulating monocytes, 2) inhibition of macrophages migration through the arterial intima, 3) enhanced uptake of low-density lipoprotein by macrophages*, en route* to foam cell formation and 4) proliferation of vascular smooth muscle cells (SMC) with consequent intimal layer thickening. When the atherosclerotic lesion becomes "vulnerable" in terms of embolic or thrombotic events, a surgical procedure is mandatory to avoid clinical consequences [1]. Even if endovascular procedures have become less invasive with shorter recovery time, percutaneous transluminal angioplasty (PTA) suffers from a high rate of restenosis (about 40% of the cases within 6 months). Moreover, stent placement, that exhibits early- and mid-term

good results data, shows long term restenosis at rates of about 30% and 12-15% in the case of bare metal and drug eluting stents, respectively [2].

Upon PTA procedures, very complex cellular processes responsible for restenosis can occur, including local reendothelialization and vascular remodeling mediated by the infiltration of a variety of inflammatory cells, cytokines, and growth factors. The pathophysiology of post-PTA restenosis involves neointimal formation that develops through three phases: thrombosis (within 24 h), recruitment (3-8 days), and proliferation of SMC, which starts on day 8 after PTA [3]. Poor reendothelialization and excessive migration and proliferation of vascular SMC in the tunica media peak at 6 months after stenting [4]. Consequently, patients at high risk of restenosis are preferentially treated with plain balloons or with drug eluting balloons (DEB) [5,6].

In general, DEB are coated with an anti-proliferative drug, mostly paclitaxel or sirolimus [7]. The treatment strategy entails that the drug is rapidly and homogenously transferred to the vessel wall during balloon inflation. However, drug lost in balloon transit or inflation may exceed 80% of the intended drug dose and crystalline/non-crystallin amorphous coatings may be associated with particulate debris, distal microembolization and downstream tissue ischemia and infarction [8]. To solve these drawbacks and improve the efficacy of the pharmacological treatment, polymeric

nanoparticles have been proposed to be administered intramurally by DEB since they can localize and sustain the drug concentration at the injured vessel [9–11]. One of the most accepted polymer family used to design implantable drug delivery systems is poly(lactide-co-glycolide) (PLGA), although there are several concerns on its use, including the formation of acidic degradation products and a moderate cytocompatibility, which in turn can lead to an intense inflammatory reaction [12] and a neointimal thickening [13–15]. A possible approach to improve PLGA biocompatibility is the grafting of antioxidant on PLGA (g-AA-PLGA). Indeed, g-AA-PLGA enabled to reduce the variation of environmental pH upon polymer degradation [16], providing antioxidant properties and improving the encapsulation efficiency of hydrophilic drugs with respect to the naïve PLGA [17].

The widely studied and used compounds to limit the risk of restenosis are anti-proliferative drugs, such as tacrolimus and sirolimus [18–21]. However, in the last years emerging evidence has been suggesting that other therapeutic agents can halt or at least slow down stenosis progression [11]. As a matter of fact, statins have effects that go beyond their mechanism of action, the so-called *pleiotropic effects* [22–25]. Besides lowering the serum cholesterol level, they possess anti-inflammatory, anti-thrombotic, anti-oxidant, and anti-mitotic effects, in addition to inhibition of

SMC proliferation [24,26,27] and matrix metalloproteinase secretion [28–30]. Preprocedural statin therapy may reduce peri- and post-PTA myonecrosis and the need for repeated revascularization; meanwhile statin-eluting stents inhibit restenosis in animal models [3,31].

This work aims to explore the potentialities of fluvastatin sodium salt (FLV) eluting nanoparticles made of caffeic acid (g-CA-PLGA) or resveratrol (g-RV-PLGA) in the prevention of restenosis. FLV appears of interest because the high-water solubility makes the encapsulation in PLGA nanoparticles and delivery to the artery wall challenging.

First, the polymer biocompatibility was studied since this feature is a key functional requirement of next-generation medical devices. Then, nanoparticle uptake was studied in SMC, endothelial cells, and macrophages, selected as representative of the cell population in blood vessel, by confocal microscopy and TEM. In this case, nanoparticles with an electrodense core were also prepared by a probe made of a combination of Ag and PVP (Ag-PVP) appositely developed. Finally, the antiproliferative potency of FLV eluting nanoparticles was investigated in cellular models.

EXPERIMENTAL SECTION

Materials

Capped poly (D,L-lactide-co-glycolide) with a co-monomer ratio of 50:50, Purasorb® PDLG 5002 (PLGA), was obtained from Corbion PURAC (NL). Caffeic acid (CA), resveratrol (RV), hydrogen peroxide (H2O2), ascorbic acid (AA), 2,2'-diphenyl-1-picrylhydrazyl radical (DPPH), poly(vinyl pyrrolidone) K30 (PVP), silver nitrate (AgNO3) and nitric acid (HNO3) were purchased by Sigma Aldrich (I); fluvastatin sodium salt (FLV) was a gift from Novartis (I). DiIC18(5)-DS (1,1'-Dioctadecyl-3,3,3',3'-Tetramethylindodicarbocyanine-5,5'-Disulfonic Acid) (DIL) was purchased from Thermo Fisher (I). All solvents were of analytical grade, unless specified.

Synthesis and characterization of g-AA-PLGA

In a 100-mL round-bottom flask, 0.5 g of PLGA were dissolved in 5 mL of THF and the obtained solution was evaporated leading to the formation of a thin polymeric film. After the addition of 50 mL of a hydrogen peroxide (H_2O_2) solution (1.0 M) and 1.2 g of ascorbic acid, the reaction was allowed to stand for 30 min. Then, the H_2O_2/AA solution was removed and replaced with 50 mL of a mixture consisting of H_2O_2 (2.0 M) and ethanol (1:1 v/v) containing 1.2 g of ascorbic acid and 0.8 mmol of the antioxidant agent (CA or RV). The reaction mixture was maintained at 25 ˚C

under atmospheric air and, after 24 h, the obtained functionalized film was purified by washing with distilled water and ethanol and dried under vacuum for 24 h at room temperature.

Polymer molecular weights were determined by using a HP1100 Chemstation (Agilent, Santa Clara, CA, USA) equipped with a combination of two columns: μStyragel™ Toluene 104 Å 7.8×300 mm and μStyragel™ Toluene 103 Å 7.8×300 mm (Waters, Milan, I). Chromatographic conditions. Mobile phase: THF; flow rate: 1.0 $mL \cdot min^{-1}$; detector: refractive index signal; injection volume: 20 μL. The molecular weight (M_w) and polydispersity index (PI) of each sample was calculated using a calibration curve made with monodisperse polystyrene standards, Mw ranging from 1,000 to 45,000 Da. A differential scanning calorimeter equipped with a refrigerated cooling system (DSC 1 Stare System, METTLER TOLEDO, CH) was used to measure the glass transition temperature (T_g). The antioxidant activity was assessed by the DPPH assay [16]. ATR-FTIR spectra were obtained using a Spectrum™ One spectrophotometer (Perkin Elmer, Monza, Italy). For this purpose, the sample under examination (~ 2.0 mg) was placed on a diamond crystal mounted in an ATR cell (Perkin Elmer, Monza, Italy). The spectra were recorded at 4 cm^{-1} resolution and 128 scans were collected over the wavenumber region 4000-650 cm^{-1}.

FLV eluting NP

Nanoparticles preparation: To prepare FLV eluting nanoparticle (NP), the drug was dissolved in the aqueous phase to get the theoretical concentration of 25% w/w. An aliquot of 0.2 mL was emulsified with 1 mL polymer solution by an ultrasonic sonotrode with tip diameter of 2 mm at 60% amplitude (Hielscher Ultrasound Technology, G) in an ice bath. The W/O emulsion was dispersed in 2.5 mL of aqueous phase under sonication in an ice bath. Then, it was diluted with 8 mL of 0.3% PVA solution and the temperature was slowly risen to 30 ˚C to favor the solvent evaporation. The loaded NP were collected by centrifugation at 11,000 rpm for 30 min at 4±1 ˚C (Universal 30 RF, Hettich GmbH & Co., G) and suspended in MilliQ® water.

Drug content: About 2 mg exactly weighed of the freeze-dried NP were incubated in 10 mL of mobile phase to extract FLV. Then the solutions were filtered through a membrane filter (pore size 0.45 μm, Millipore, I) before HPLC measurements. The experimental FLV loading (as %) and the encapsulation efficiency (EE, %) were calculated. All operations were carried out away from light.

In vitro FLV release: The release studies from NP were conducted in triplicates using dialysis membrane made of regenerated cellulose with a MWCO = 8-10 kDa (Float-A-Lyzer G2, ThermoFisher, I) loading 5 mL of nanosuspension. The dialysis tube was immersed in 19 mL of pH 7.4 BPS at 37±1 ˚C under magnetic stirring at 1600 rpm. At predetermined time points, 200

μL of the release medium was withdrawn and replaced with fresh buffer. At the end of experiment, the nanosuspension was centrifuged twice at 10,000 rpm for 30 min; the supernatants withdrawn, and the pellet was dissolved in mobile phase to extract the remain drug. The diffusion profile of the pure FLV was also obtained using the same testing conditions.

HPLC method: The drug quantification was carried out using an HPLC (HP1100 series, Agilent, UK), equipped with a quaternary pump, an auto-sampler, a thermostated column compartment at 25.0±0.1 ˚C and DAD-UV detector. An aliquot of 10 μL was eluted through a C18 column (Phenomenex Luna®, LC 5 μm, 150 × 46 mm) using a mixture of acetonitrile / pH=3.0 phosphate buffer (60:40 % v/v) at the flow rate of 1.2 mL/min. The detection of FLV was performed at 230 nm. Calibration curve in the range of 1-50 μg/mL (R^2>0.99).

Fluorescent NP

Placebo and fluorescent NP were prepared by nanoprecipitation using a lab-scale membrane emulsification system (Micropore LDC-1, Micropore Technologies Ltd, UK) equipped with a stirred cell. Briefly, a solution constituted of 1% PLGA or g-AA-PLGA in acetone (2 mL) was loaded into a disposable syringe connected to a syringe infusion pump (Aladdin AL300, UK). The organic phase was pushed at the rate of 0.1 mL/min through the pores of a precision engineered

stainless steel membrane into 25 mL MilliQ® water, while a paddle, positioned above the membrane and stirred at 1000 rpm, induced a shear force which results in droplet detachment. The dispersion was left under stirring for 2 h to evaporate the solvent. FITC-NP were similarly prepared, using 10% w/w of FITC-PLGA [32]. In the case of DIL, the polymer solution was mixed with 0.01% DIL-in methanol in volume ratio 1:0.0025 before injection.

NP were characterized in terms of size and zeta potential using a Zetasizer Nano ZS DLS instrument (Malvern Instruments, UK) at 25.0±0.1 ˚C and DIL loaded NP were also characterized at 565 nm long-pass filter both in scattering and fluorescent mode using a Nanoparticle Tracking Analysis (NTA, Malvern Instruments, UK) and their stability, expressed in terms of size distribution and concentration, was monitored over a 10-day period.

Electron-dense NP

Ag-PVP probe was prepared as follows: 50 mg of silver nitrate were dissolved in 10 mL of distilled water; then, 1 g of PVP was added and the solution was stirred overnight at room temperature. The obtained solution was introduced into dialysis tubes (molecular weight cut-off, MWCO: 12-14000 Da, supplied by Medicell International Ltd, London, UK) and dipped into a glass vessel containing

distilled water at room temperature for 24 h with four changes of water. Finally, the resulting solution was frozen and dried with a Freeze Dryer Micro Modulo (Edwards, UK).

The silver content of the prepared Ag-PVP probe was evaluated by digesting the sample with 70% HNO_3 in a microwave at 150 ˚C for 10 min [33]. Then, the digested sample was diluted with distilled water to reduce the HNO_3 concentration to 3.5%. The silver concentration was evaluated by inductively coupled plasma mass spectroscopy (ICP-MS) (PerkinElmer Elan DRCII).

Nanosuspension was obtained as described in section 2.4 using an organic phase constituted of PLGA or g-CA-PLGA and Ag-PVP in the ratio from 1:9 to 3:7. The morphology of electrondense nanoparticles was assessed by TEM.

Cells

The human smooth muscle cell (SMC) line was purchased from ATCC, USA (PCS-100-012) and were used between the fourth and the seventh passage. The culture medium used is ATCC Vascular Cell Basal Medium, added with 500 µl of ascorbic acid, 500 µl rh EGF, 500 µl rh insulin and rh FGF-b, 25 ml of glutamine, 25 mL of FBS (ATCC Vascular Smooth Muscle Growth Kit) and 5 ml of Penicillin-Streptomycin 100X (Euroclone, Milan, I).

The human endothelial EA.hy926 cell (EHEC) line (ATCC CRL-2922, USA) was cultured in high glucose Dulbecco's modified Eagle's medium (DMEM; EuroClone, I) supplemented with 10% Fetal Bovine Serum (FBS), 2mM L-Glutamine, 100 U/mL penicillin, 100 μg/mL streptomycin, and 2% HAT supplement (Sigma Aldrich, I).

The human monocyte-derived macrophages were isolated from the blood of healthy volunteers and cultured in with DMEM containing 10% human AB serum and insulin (8 μg/mL).

MTT assay

Cellular toxicity caused by g-AA-PLGA NP was assessed both by measuring cellular protein content and by using the 3-(4,5-dimethylthiazol-2-yl)-2,5-diphenyltetrazolium bromide) (MTT) colorimetric assay which relies on the ability of viable cells to actively metabolize the dye. Briefly, after incubation with NP (100 μg/mL) for 24 h, cells were washed with PBS and MTT (Sigma-Aldrich, I) was added at a concentration of 10 μg/mL in the culture medium. Following 90 min of incubation, the supernatants were discarded, the intracellular formazan precipitates were solubilized by the addition of 100% DMSO and plates placed on a plate shaker for 10 min. Absorbance was evaluated at 620 nm. A 4% solution of Triton was used as positive cytotoxic control.

Cellular uptake of NP

Cellular uptake of fluorescent PLGA, g-CA-PLGA and g-RV-PLGA NP was evaluated in human SMC, macrophages and endothelial cells. Briefly, cells were seeded at the cellular density of 30,000 cells/well in a 96-well plate. After reaching the confluence, cells were washed with PBS and the culture medium with 0.2% EFAF containing the fluorescent NP at a final concentration of 100 μg/mL was added. Incubation times were 0.5, 2 and 4 h for macrophages and 4, 16 and 24 h for SMC and endothelial cells. After the incubation period, plates were cooled with ice, media were removed, and cells were washed three times with cold PBS and fixed with methanol for 20 min. After methanol removal, cells were washed again three times with PBS. Culture medium without NP was used as negative control. A microplate reader (Wallac 1420 Victor^2 Microplate Reader, PerkinElmer, I) was used to measure the fluorescence intensity from up-taken NP in each well at 25.0±0.1 ˚C, with lamp filter and emission filter at 535 and at 485 nm, respectively. The cellular uptake efficiency was calculated normalizing the observed fluorescence intensity in each well (I_{OBS}) by the mean fluorescence intensity of the negative control (I_{NC}), as reported in **Equation 1:**

$$Relative\ fluorescence\ (\%) = \frac{I_{OBS} - I_{NC}}{I_{NC}} \times 100 \qquad \textbf{Equation 1}$$

Only the samples with a fluorescence higher than the highest fluorescence registered for the negative control were used for the analysis. Results are reported as mean ± SEM (n=6).

TEM analysis

The uptake of NP and their distribution inside the three cell lines were deepened by transmission electron microscopy (TEM) using Ag-NP in order to assure a simpler recognition. Macrophages, endothelial cells and SMC were seeded at cellular density of 300,000 cells in 35-mm diameter Petri dish and incubated for 96 h. Cells were then washed with PBS and treated for 4 h with placebo g-CA-PLGA NP diluted with MEM + 0,2% EFAF (MEM + 0,2% EFAF without NP was also used as negative control). After washing with PBS, cells were detached with trypsin and centrifuged at 1,500 rpm for 15 min. Pellets were washed with 0.1 M sodium cacodylate buffer at pH 7.3 and centrifuged twice, as previously reported. Pellets were fixed overnight in a solution containing 2% of freshly prepared paraformaldehyde and 2% glutaraldehyde in 0.1 M sodium cacodylate buffer at pH 7.4. Samples were rinsed twice in the same cacodylate buffer for 30 min and post-fixed in 1% osmium tetroxide in cacodylate buffer 0.1 M at 0 ˚C for 90 min. Pellets were then washed in distilled water followed by a staining with 2% aqueous uranyl acetate, dehydrated in a graded acetone series and embedded in Epon-Araldite resin. Ultrathin sections were cut by a Leica

Supernova ultramicrotome (Reichert Ultracut, Wien, Austria) and counterstained with lead citrate. TEM was performed with a Zeiss EM10 electron microscope (Carl Zeiss, Oberkochen, Germany).

Confocal analysis

Human SMC were seeded at a density of 10^5 cells *per* well in 200 µl of DMEM media on µ-Slide eight-well glass-bottom dishes (ibidi, GER). After 24 h, ~$3x10^9$ DIL-labelled NP (PLGA or g-CA-PLGA) were added in each well and cells were incubated for up to 24 h. Next, the cells were washed 3 times with PBS to remove NP not internalized, fixed with paraformaldehyde 4% at room temperature for 10 s, washed 3 times with PBS, and stained at room temperature for 5 min with a solution of Cellmask deep red (Invitrogen, US) and Hoechst 33342 (Invitrogen, US), both at a final concentration of 2 µg/ml. After final washing, the cells were imaged using a confocal microscope (Leica Stellaris, GER) with either a 40× air or 63× glycerol objective. Quantification of DIL fluorescence *per* cell and *per* field of view were measured by processing raw data with NIS-Elements v.5.2 digital imaging analysis software (Nikon Instruments, JAP) for segmentation and precise quantification, implementing the general-analysis tool-box.

Evaluation of cell proliferation and migration

In order to evaluate the effect of free and NP encapsulated FLV on cell proliferation, SMC and endothelial cells were seeded at 5,000 cells/well in a 12-well plate until confluence. Cells were treated with FLV dissolved in ethanol and FLV-NP at the drug concentration of 1, 2, 4, 6, 10 μM, using ethanol and placebo NP as negative controls. After the removal of the treatments, cells were detached with trypsin and counted with a Coulter Counter (Z1 Beckman Coulter, I), calibrated at the threshold of 6.8 μm. Results are reported as mean ± SEM (n=6).

For the evaluation of cell migration, the *in vitro* scratch wound method was used. Human SMC and endothelial cells were seeded at the density of 5,000 cells/well in a 12-well plate and incubated in media until confluence was reached. After a washing step with PBS, fresh medium was added before treatment. A wound in cellular monolayers was made by using a sterile disposable tip and detached cells were removed by washing with PBS. Then, cells were incubated for 24 h with increasing concentrations (2, 4 and 10 μM) of FLV-NP and the matching concentrations of either placebo NP or FLV solution in ethanol (vehicle). Cell directional migration was evaluated by measuring cell ability to reclose the wounded area by using phase-contrast microscope and photographed using a digital camera (Axiovert 200, Zeiss, G). Images were acquired after 24, 48, 72 and 144 h. For quantitative representation of the results, the percentage of reclosure of the

scratched area in the monolayer was determined by using Axiovision software (Zeiss, USA). Results are reported as mean ± SEM (n=6).

Statistical analysis

One-way and two-way analysis of variance (ANOVA) followed by Tukey's test as post ANOVA means comparison were performed using OriginPro® 2015 (OriginLab Corporation, USA), considering the different type of polymer and the time of incubation with cells as factors. Differences were considered statistically significant at a level of α=0.05. Outliers were discarded according to Dixon's T-test.

RESULTS AND DISCUSSION

Synthesis and characterization of g-AA-PLGA and Ag-PVP

In the present study, antioxidant grafted PLGA (g-AA-PLGA) was prepared according to a free radical grafting approach involving two main reaction steps and the use of ascorbic acid/hydrogen peroxide redox pair.

In the first step of the reaction, the initiator system generates radical species that react with PLGA leading to the formation of macroradicals; the following step involves the insertion of the antioxidant molecules, such as caffeic acid or resveratrol, onto the polymeric chain through the formation of covalent bonds. In a previous study[17], it was hypothesized that hydroxyl radicals, resulting from the oxidation of ascorbic acid in the presence of hydrogen peroxide, activated PLGA initiating the grafting reaction. A further study highlighted a different reaction mechanism mediated by ascorbate radicals ($Asc^{\bullet-}$) [34].

Ascorbic acid (AA), indeed, is susceptible to autoxidation in water solution, due to the presence of two ionizable hydroxyl groups, with the generation of ascorbate radicals. In detail, the dissociation of 3-OH and 2-OH leads to the formation of ascorbate monoanion ($AscH^-$) and ascorbate dianion (Asc^{2-}). The first one, which is an excellent reducing agent, undergoes two successive one-electron oxidations producing ascorbate radical and, finally, dehydroascorbic acid. The AA autoxidation is accelerated by the presence of hydrogen peroxide with a higher $Asc^{\bullet-}$ production according to the mechanism reported in **Figure 1A** [35].

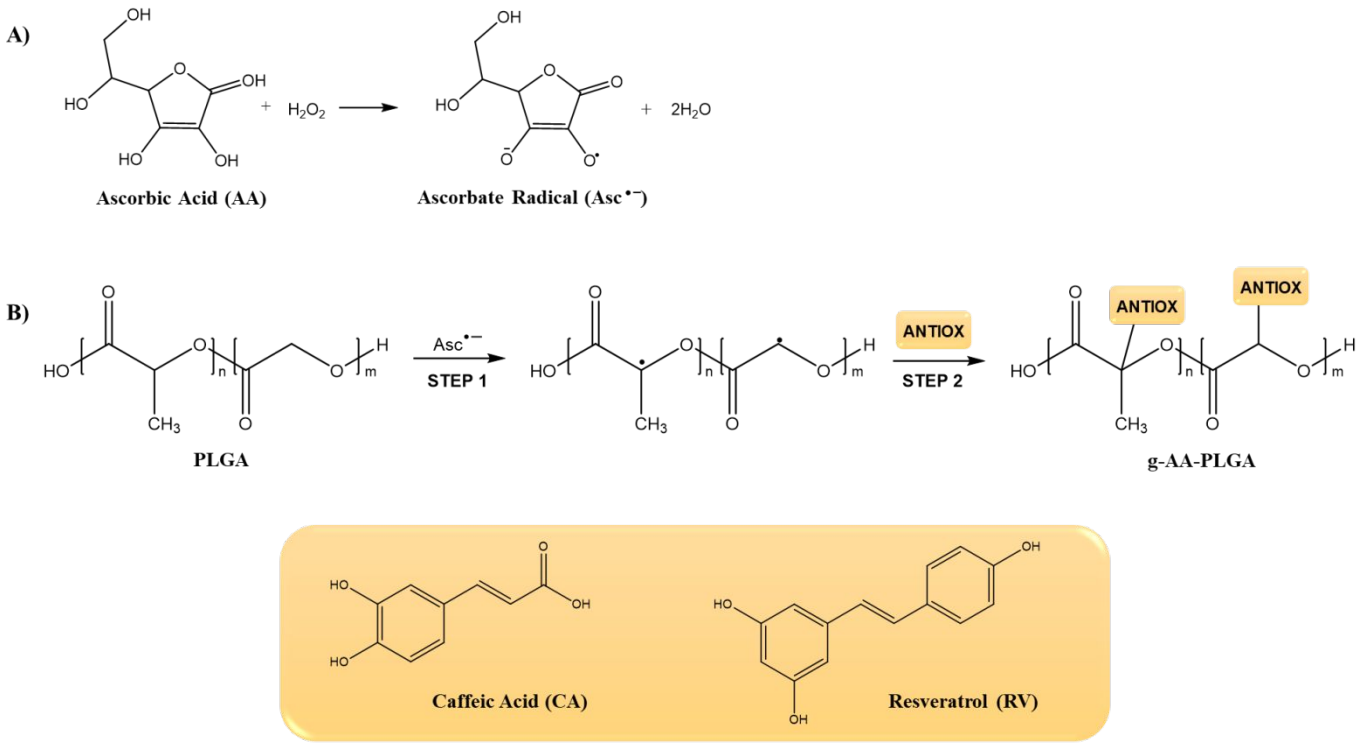

Figure 1. A) Ascorbic acid/hydrogen peroxide reaction mechanism and **B)** reaction scheme for the synthesis of g-AA-PLGA.

The so formed ascorbate radicals react with PLGA to abstract hydrogens on carbons alpha to carbonyl groups forming macroradicals (**Figure 1B**). The subsequent step involves the reaction of the macroradicals active sites with the ortho- and para- positions relative to the hydroxyl groups of the antioxidant compounds leading to the insertion of these molecules onto PLGA backbone [36,37].

The main features of PLGA and g-AA-PLGA raw materials are summarized in **Table 1**. The data confirmed the suitability of the synthetic strategy, which permits the conjugation of caffeic acid or resveratrol on the copolymer backbone without a consistent modification of M_w and T_g. Furthermore, the comparison of the data with those obtained in a previous work confirmed the good reproducibility of this mild grafting technique [17]. DPPH assay was conducted to evaluate whether resveratrol and caffeic acid retained their antioxidant capacity after grafting on PLGA backbone. As expected, the control polymer did not show any antioxidant activity, while g-CA-PLGA exhibited a higher radical scavenging activity with respect to g-RV-PLGA (**Table 1**).

Table 1. Physico-chemical features of g-CA-PLGA and g-RV-PLGA and their antioxidant properties expressed as DPPH radical inhibition (%).

Polymer	M_w (KDa)	PI	T_g (°C)	DPPH radical inhibition (%)			
				1 h	2 h	3 h	24 h
PLGA	20.4	1.52	35.8	0±0.4	0±0.4	0±0.5	0±0.3
g-CA-PLGA	18.4	1.65	34.5	90±0.4	92±0.7	93±0.6	97±0.6

g-RV-PLGA	18.5	1.38	34.8	27±0.8	32±0.4	37±0.3	56±0.5

The Ag-PVP probe, obtained by the chelation of silver by PVP oxygen and nitrogen atoms, presented a monomodal distribution with a hydrodynamic diameter (expressed as volume) of about 12 nm. Inductively coupled plasma mass spectrometry (ICP-MS) was employed to evaluate the silver content of Ag-PVP and the performed analysis revealed a silver content equal to 11.8 mg/g. This complex was designed since Ag guarantee an electrondense signal in TEM analyses of biological sample and PVP, as a hydrophilic portion, assures a good dispersibility in water and methylene chloride and a suitable stability of the dispersed system nanoparticles.

Characterization of NP

The different physico-chemical characteristics of NP components required the adoption of different preparation methods. In all cases, the experimental set up allowed the obtainment of monodispersed NP with similar hydrodynamic diameters (D_H) and negatively charged with zeta potential of about -30 mV (**Table 2**).

Table 2. Main features of different types of NP.

Form ID	Main constituent(s)	FLV (%)	D_H (nm)	PdI	ζ (mV)
PLGA-NP	PLGA	-	186±1	0.061±0.016	-32.4±0.6
CA-NP	g-CA-PLGA	-	171±2	0.082±0.020	-30.4±1.0
RV-NP	g-RV-PLGA	-	193±3	0.064±0.016	-32.5±0.6
F-PLGA-NP	PLGA/FITC-PLGA (10%)	-	172±1	0.090±0.017	-29.7±0.4
F-CA-NP	g-CA-PLGA/FITC-PLGA (10%)	-	176±1	0.087±0.015	-30.0±0.2
F-RV-NP	g-RV-PLGA/FITC-PLGA (10%)	-	185±1	0.083±0.013	-29.4±0.6
Ag-PLGA-NP	PLGA /Ag-PVP (20%)	-	172±1	0.143±0.024	-29.1±0.9
Ag-CA-NP	g-CA-PLGA/Ag-PVP (20%)	-	230±3	0.253±0.008	-17.4±0.3
FLV-PLGA-NP	PLGA	4.5±0.7	175±3	0.125±0.045	-33.1±0.3
FLV-NP	g-CA-PLGA	10.6±1.0	185±1	0.133±0.028	-28.4±2.1
FLV-RV-NP	g-RV-PLGA	9.1±2.0	180±2	0.145±0.018	-29.7±1.2

Next, we assessed the biocompatibility of placebo NP on macrophages, endothelial cells and SMC representatives of the main cell types present in the vessel wall. Overall, the grafted polymers were well tolerated by all cell lines, as not-significant differences in cell viability were observed

compared to control culture medium alone (control, **Figure 2A**). This suggests that the antioxidant-based grafting does not affect the *in vitro* cytotoxicity of PLGA.

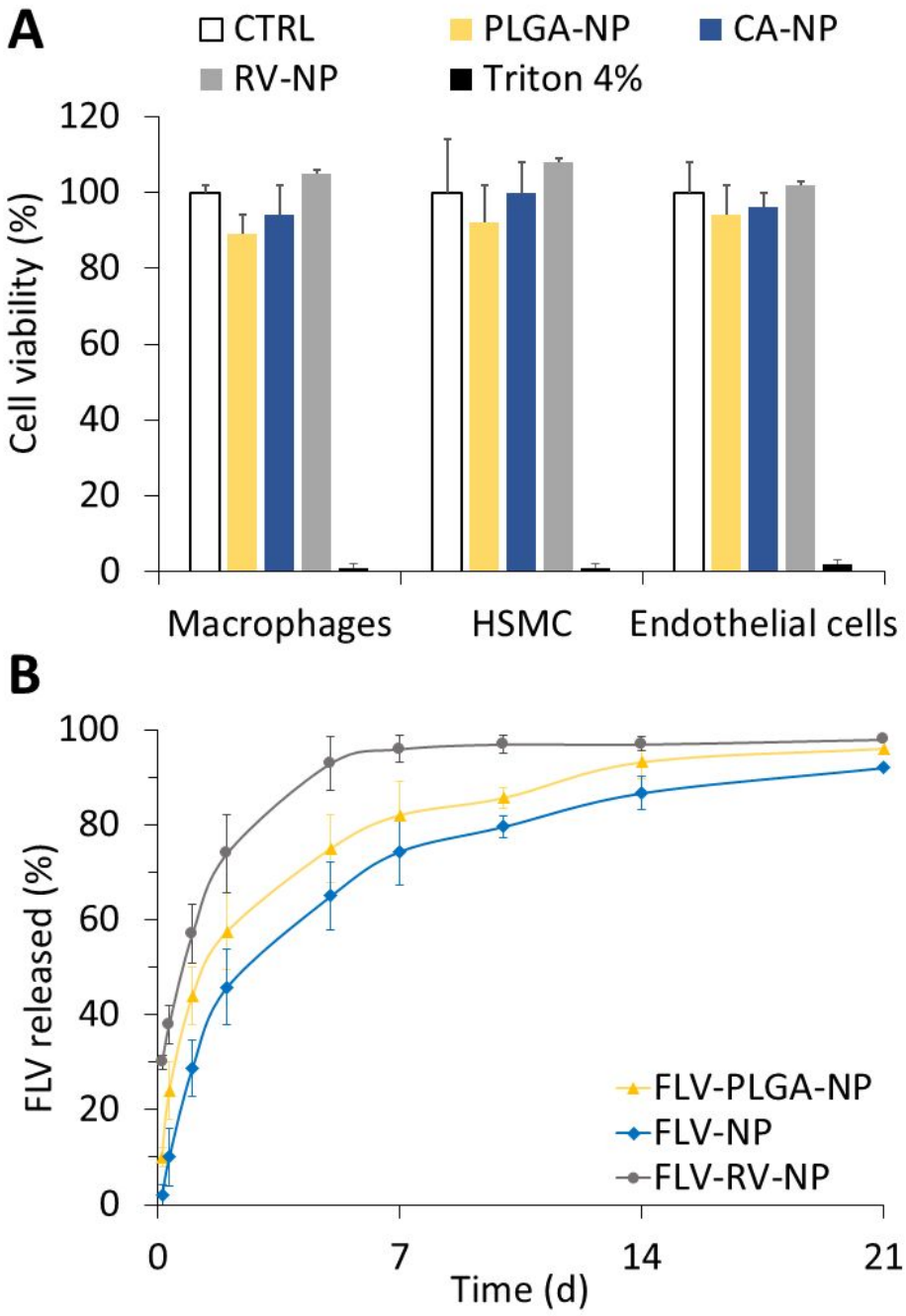

Figure 2. panel **A**) Cell viability after 24 h of incubation with the NP. Panel **B**) *In vitro* release profiles of fluvastatin from NP made of PLGA (FLV-PLGA-NP), g-CA-PLGA (FLV-NP) and g-RV-PLGA (FLV-RV-NP).

The further modification of the preparation method required to encapsulate high-water soluble FLV into polymeric NP, did not affect NP main features. As expected by previous experience with ovalbumin [17], the use of g-AA-PLGA allowed the loading of a double amount of FLV (**Table 2**).

However, the drug release profile obtained with the two grafted copolymers were different. FLV-RV-NP gave a high burst effect since about 30% FLV was released at early data points and the plateau was reached in about 7 days (**Figure 2B**). As in the previous case, the FLV burst effect was higher for PLGA NP (i.e. about 10%) compared to the g-CA-PLGA, which was considered negligible. Nevertheless, the drug release rate constants, calculated according to Higuchi's equation (K), overlapped (FLV-PLGA-NP: K=0.341±0.010 d^{-1}; FLV-NP: K=0.337±0.012 d^{-1}) and a prolonged release of FLV was assured beyond 3 weeks for both formulations.

To evaluate the internalization by the different cell types present in the arterial wall, NP made of grafted polymers and with different features were prepared. Specifically, NP loaded with FITC or DIL to be used for fluorescence imaging, or electrondense NP to be employed for TEM

assessments. NP containing 10% w/w FITC-PLGA maintained the same features of the placebo NP (**Table 2**) and were, therefore, used to estimate the cellular uptake in the three cell lines. Nevertheless, FITC signal is subject to high quenching and, therefore, NP loaded with DIL were preferred for confocal imaging. In this latter case, some preliminary experiments were carried to optimize the probe:copolymer ratio and the selection of organic solvent(s) to obtain NP by using the solvent displacement method. To avoid aggregation, the solution containing 0.01% DIL in methanol was mixed to the PLGA solution in acetone. The slight reduction in surface charge from -30 mV to about -4 mV in DIL-PLGA-NP was due to the probe adsorption on the NP surface. This data was supported also by the slight increase of particle size distribution derived from NTA analyses after the activation of a 565nm-long pass filter for green laser. Indeed, the non-fluorescent PLGA-NP showed a D_{50}=117±2 nm and D_{90}=174±11 nm which shifted toward D_{50}=135±2nm and D_{90}=208±3 nm in the case of the fluorescent PLGA-NP. These values did not undergo any variations over a 10-day period of time, (t_0: $6.85\times10^{10}\pm2.86\times10^{8}$ particle/mL; t_{10}: $7.03\text{x}10^{10}\pm8.40\text{x}10^{8}$ particle/mL; D_{50}=136±2 nm; D_{90}=214±1 nm) confirming the stability of the labeling. Similarly, DIL-CA-NP presented a monotonic dispersion (D_{50}=150±5 nm and

D_{90}=226±212 nm) and a similar concentration ($3.34\times10^{10}\pm1.23\times10^{9}$ particles/mL) which did not significantly change over 10 days of storage at 4 ˚C.

Finally, electron dense NP (Ag-PLGA-NP and Ag-CA-NP) were designed to properly distinguish the polymeric constructs from cellular organelles in TE microphotographs. The loading of 20% Ag-PVP was considered optimal since NP presented a well-defined core surrounded by a PLGA wall (**Figure 3B**). Conversely, NP with lower Ag content resulted inhomogeneous with a pale core (**Figure 3A**), and those loaded by the greatest amount resulted completely electrodense (**Figure 3C**).

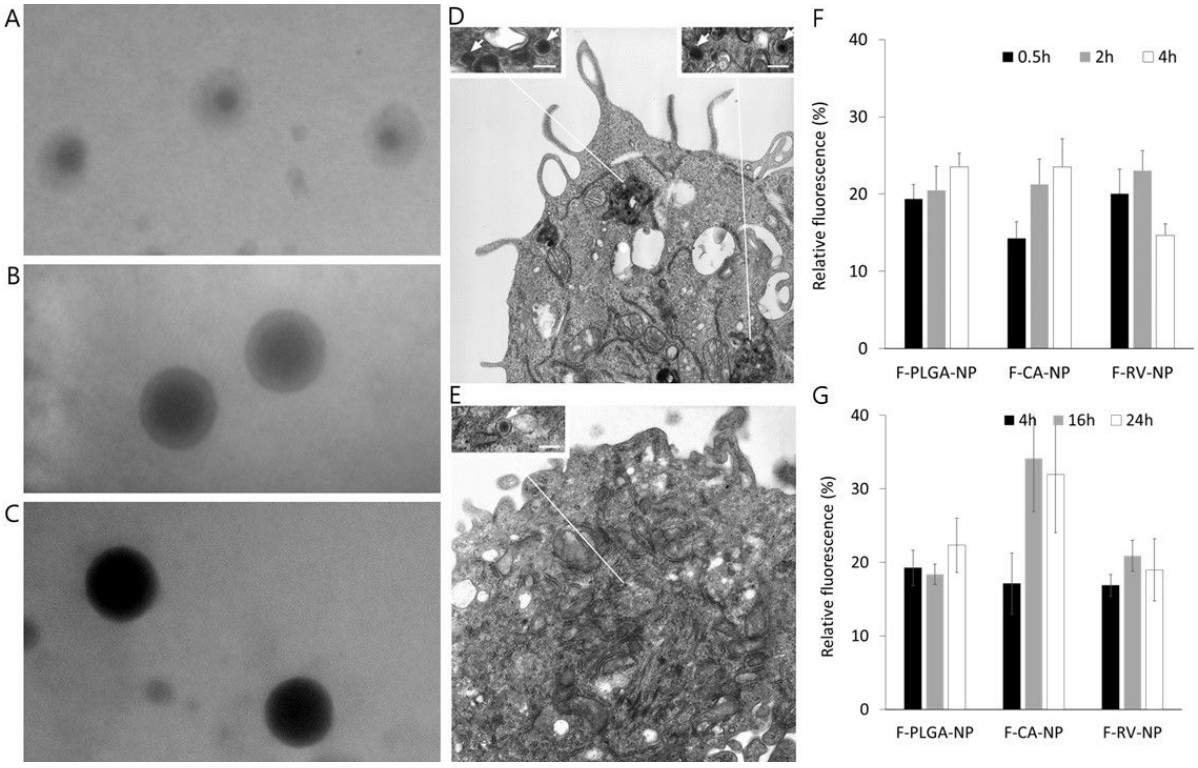

Figure 3. The Ag-PVP conjugate loading in NP ranged from 10 to 30% w/w without influencing the hydrodynamic diameter and PDI (D_H ~ 280 nm). To optimize the conjugate content, NP were observed by TEM. At 10% loading, the electrodense core was not uniformly defined (panel **A**); whilst at the highest content, the entire NP appeared dark (panel **C**). Only at 20% loading, it was possible to clearly detect an electrodense core surrounded by a PLGA wall (panel **B**). This peculiar structure allowed also discriminating among NP if Ag-PVP loaded NP were mixed by blank NP at a 1:1 ratio. Panel **D** reports a representative TE micrograph showing a macrophage containing within the cytoplasm a large phagosome. Arrows point at some NP between the ingested material.

Scale bar: 100 nm. Panel **E** shows a typical TE micrograph of an endothelial cell showing a single NP particle (arrow) dispersed within the cytoplasm. Scale bar: 100 nm. Finally, panels **F** and **G** report the uptaken PLGA-NP, F-CA-NP and F-RV-NP in macrophages and endothelial cells, respectively.

Uptake of placebo NP

We determined the uptake of NP made of different copolymers by macrophages, SMC and endothelial cells, to provide provisional data on the amount of NP which could be potentially retained in the vessel wall after administration by DEB. We also included the contribution of NP adsorbed on the cell surface and entrapped in the extra-cellular space which also can contribute to the availability of FLV since they assure the release of the drug over a prolonged period of time. As expected, NP were taken up faster by macrophages compared to the other cell lines, as intracellular fluorescence was already detectable after only 30 min of exposure (**Figure 3F**). Moreover, the grafting of caffeic acid or resveratrol on the PLGA backbone did not influence the uptake process, independently of the incubation time (Two-way ANOVA, $p>0.05$) (**Figure 3F**).

In the case of endothelial cells, after 16 h of exposure to the NP, the fluorescence in the cells treated with F-CA-NP resulted significantly higher than in those treated with F-PLGA-NP or F-

RV-NP (One-way ANOVA followed by Tukey's test, F-CA-NP *vs* F-PLGA-NP (p=0.028) and F-CA-NP *vs* F-RV-NP (p=0.032), **Figure 3G**).

On the contrary, SMC took up F-CA-NP more rapidly than the other two formulations, (One-way ANOVA followed by Tukey's test, F-CA-NP *vs* PLGA-NP p=0.002, F-CA-NP *vs* F-RV-NP p=0.004 and F-RV-NP *vs* PLGA-NP p=0.984, **Figure 4A**). Afterwards, a significant decrease in the relative fluorescence (%) was observed only for F-CA-NP. Considering that no cytotoxic effects were detected over a 24h-period, the reduced ability to sustain the NP uptake can be due to the beginning of exocytosis, as already reported in literature [38]. Conversely, no statistical differences were found in NP concentration over time for the other two formulations (**Figure 4A**). Considering (i) the poor ability of g-RV-PLGA to control the FLV release and that (ii) no statistical differences in the uptake of PLGA-NP were observed in all cell lines, this polymer was discarded from further evaluations.

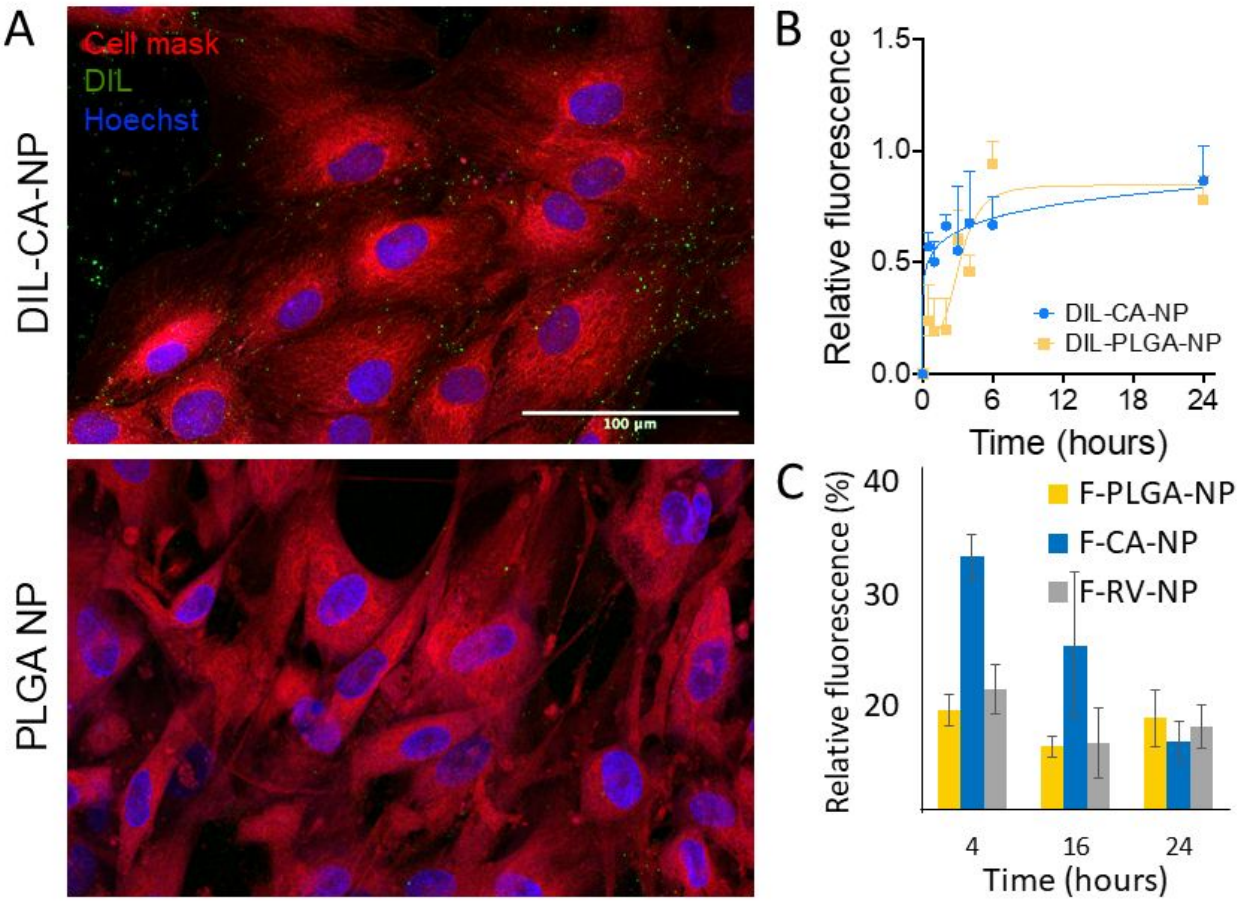

Figure 4. Panel **A** shows representative images of SMC incubated for 1 h with either DIL-CA-NP or DIL-PLGA-NP and imaged by confocal microscopy. Panel **B** reports quantification of the intracellular fluorescence measured on single cells over 24 hours (mean ± SD). Panel **C** is related to the uptake of PLGA-NP, F-CA-NP and F-RV-NP in SMC at different time points.

The deeper insight using TEM revealed that the different distribution of NP in the cell lines was independent of the polymer. The most distinctive feature is the presence of endocytotic vesicles, lysosomes, and phagolysosomes within the cytoplasm of macrophages (**Figure 3D**), which is a fingerprint of such professional phagocytes. In this case, we evidenced the presence of some internalized NP interposed between other ingested material (**Figure 3D**). The ability of the other two cell lines to uptake NP appears different since single Ag-CA-NP particles were found to be dispersed in the cytoplasm as exemplified in **Figure 3E** for endothelial cells.

We decided to further investigate the internalization of both DIL-PLGA-NP and DIL-CA-NP by SMC because FLV should inhibit their proliferation which is one of the main causes of restenosis. SMC were cultured with both NP at different incubation times, ranging from 0.5 to 24 hours, and then imaged by confocal microscopy (**Figure 4A)**.

The results demonstrate that NP were rapidly internalized and accumulated inside the cells as a function of time, regardless of the presence of the CA on the PLGA backbone. Overall, the fluorescent signal observed was punctiform and widely distributed across the cell cytoplasm. We further performed image analysis on single cells to quantify the relative fluorescence associated to the dye. The measurements revealed that, over the first 6 h of incubation, DIL-CA-NP had a faster

dynamic of internalization compared to the pristine preparation (**Figure 4B**). The quantification of the relative intracellular fluorescence suggests that the presence of caffeic acid in g-CA-PLGA could favor the initial binding of the NP to the SMC promoting a rapid internalization, as verified in the set of experiments performed using FITC PLGA conjugate as a probe (**Figure 4C**).

Thus, on the bases of all data, g-CA-PLGA was selected as the most promising material for the *in vitro* studies on cell proliferation.

Effect of FLV-NP on human SMC and endothelial cell proliferation and migration

To test the efficacy of NP loaded with FLV in inhibiting SMC proliferation, human SMC and endothelial cells were incubated with increasing concentration of FLV-NP for 24 h, and with the matching concentrations of either the placebo NP or a FLV solution.

As expected [39], the drug alone inhibited SMC proliferation in a statistically significant manner starting at concentrations higher than 1.2 μM (at 2 μM cell proliferation was inhibited by 100%) (**Figure 5A**).

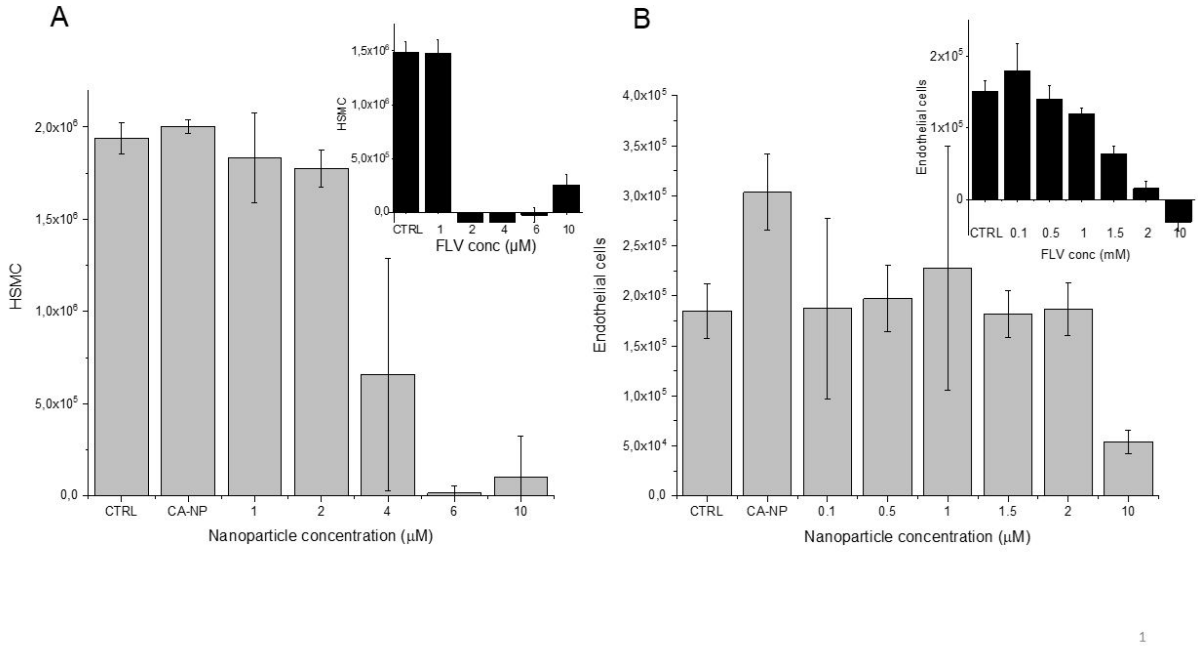

Figure 5. Effect of FLV-NP and fluvastatin (insert) on (**A**) human SMC proliferation and (**B**) endothelial cells proliferation.

FLV-NP were also effective in inhibiting SMC proliferation: at 4 μM and 6 μM cell proliferation was reduced by 50% and 100%, respectively (**Figure 5B**). This demonstrates that NP efficiently delivered the encapsulated drug to cells and that the drug was still pharmacologically active and able to affect cell behavior.

In endothelial cells, the addition of FLV resulted in a concentration-dependent and statistically significant reduction of cell proliferation, with the maximal inhibitory effect achieved at a

concentration of 1.5 μM (**Figure 5C**). On the contrary, the incubation with FLV-NP did not affect endothelial cell proliferation, except for the highest concentration tested (10 μM, **Figure 5D)**. Surprisingly, the addition of the placebo NP stimulated the endothelial cells proliferation by about 50% (**Figure 5D**).

Finally, the effects of FLV-NP on cell migration were analyzed by using the directional migration assay [40].

The drug alone and the FLV-NP reduced human SMC directional migration in a concentration and time-dependent manner (up to 80% inhibition at the longest time-point tested, **Figure 6**). Enhanced migration of human SMC with an almost completed wound closure was evident after 144 h when cells were treated with the vehicle alone, indicating that they preserved the motility in our experimental conditions. Similar results were obtained after the treatment with placebo NP. When cells were treated with FLV alone or with FLV-NP, a significant area of the wound remained not covered.

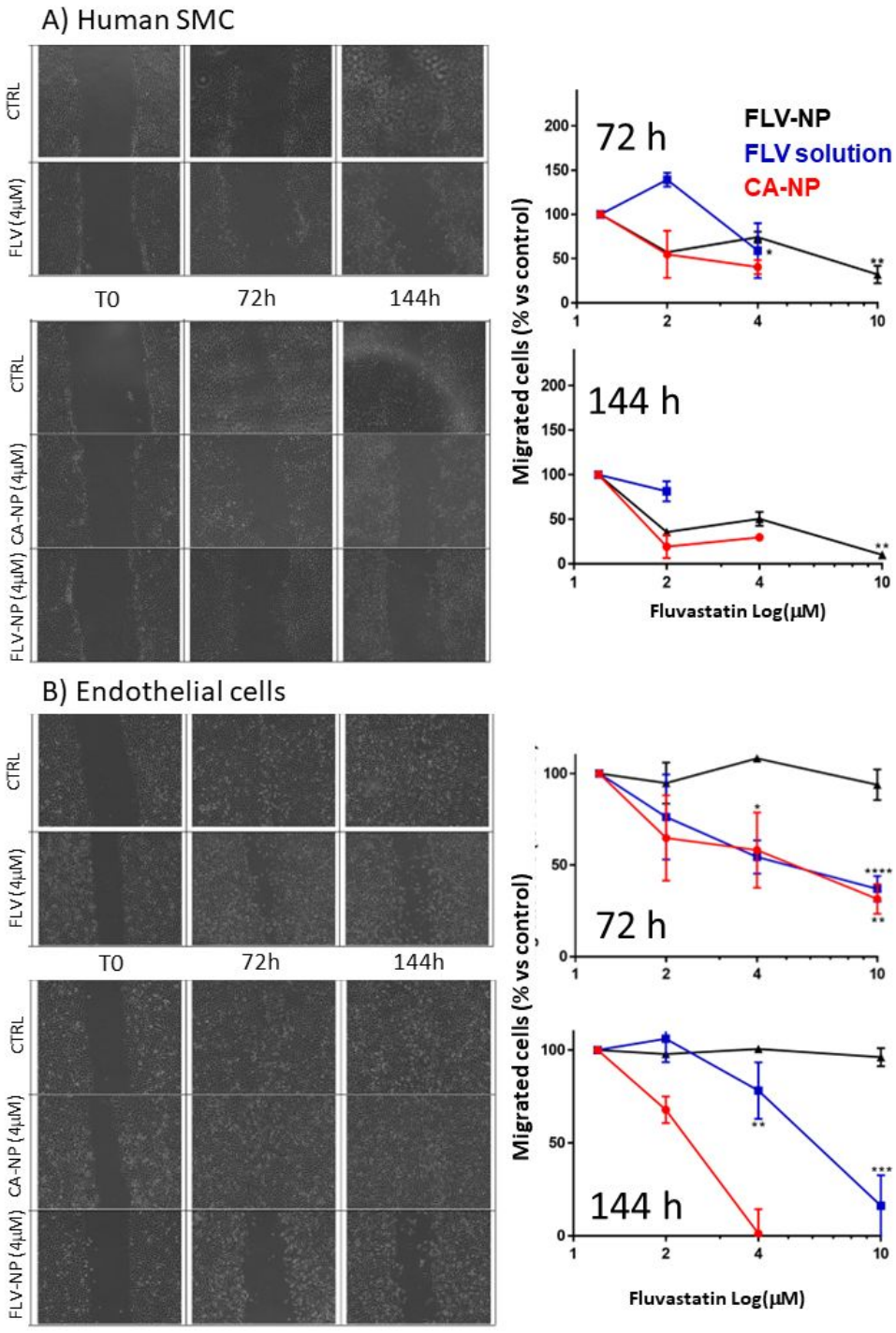
A) Human SMC
CTRL
FLV (4μM)
T0
72h
144h
CTRL
CA-NP (4μM)
FLV-NP (4μM)
72 h
FLV-NP
FLV solution
CA-NP
Migrated cells (% vs control)
144 h
Fluvastatin Log(μM)
B) Endothelial cells
CTRL
FLV (4μM)
T0
72h
144h
CTRL
CA-NP (4μM)
FLV-NP (4μM)
Migrated cells (% vs control)
72 h
144 h
Fluvastatin Log(μM)

Figure 6. Effect of fluvastatin and FLU-NP on directional migration of **A**) human SMC and **B**) endothelial cells at different time points. Black: CA-NP; red: FLV solution; Blu: FLV-NP. (*p<0.05; **p<0.01; *** p<0.001; ****p<0.0001 vs CTRL).

The addition of FLV alone and of FLV-NP reduced in a concentration and time-dependent manner also endothelial cell migration. The placebo NP did not affect this process (data no shown). After the treatments with vehicle, culture medium (negative controls), or CA-NP, the wound areas were completely reclosed, while in the presence of FLV alone or FLV-NP the wound areas were still uncovered at the latest time point, particularly evident in the case of FLV-NP.

All together the data show that g-CA-PLGA may assure a prolonged release of FLV in a pharmacologically effective form. Indeed, upon administration of NP in the injured vessel, the drug release can be assured by two different mechanisms: the diffusion from NP adsorbed in the extracellular matrix and the cellular uptake. Indeed, the data demonstrated that the FLV-NP effectively enter into SMC, endothelial cells and macrophages. In particular, a concentration and time-dependent inhibition of human SMC proliferation was observed after treatment with FLV-NP, with a 50% inhibition at 4 μM and the maximal effect at 6 μM. As expected, this effect is achieved at a FLV-NP concentration slightly higher than what we obtained by the direct addition

of FLV to cells that completely abolished SMC proliferation at a concentration of 2 μM. In the case of endothelial cells, FLV blocked the proliferation in a concentration-dependent manner. Conversely, when the drug was delivered by FLV-NP, no inhibitory effect on the endothelial cells was observed, except at the highest concentration tested (10 μM) which most probably highlights a toxic effect on the cell monolayer. Of note, the addition of placebo NP resulted in a stimulation of endothelial cells proliferation by about 30%, while no effect was observed on SMC. All together these data suggested that the encapsulation of FLV in g-CA-PLGA NP seems to improve a selectivity of the drug towards SMC rather than endothelial cells.

Regarding the effects on proliferation, FLV-NP inhibited the directional migration of human SMC in a concentration-dependent manner, achieving its maximal inhibitory effect already after 48 h of incubation at the highest concentration tested (data not shown). At later time points (72 and 144 h), at the 2 μM concentration the FLV-NP resulted more efficacious in inhibiting the SMC migration with respect to the FLV solution (**Figure 6A**) confirming the beneficial of assuring a prolonged release by NP. It should be also underlined that placebo NP became cytotoxic at the highest concentration (CA-NP, **Figure 6A**) suggesting a synergic effect of g-CA-PLGA and FLV. This cytotoxic effect of placebo NP was not detected in the case of endothelial cells and the ability

of FLV-NP to inhibit the directional migration overlapped with that of FLV solution within the 72 h. At the longest time points, the FLV-NP resulted more effective independently of the tested concentration suggesting that the control of the drug release played a key role in endothelial cell migration (**Figure 6B**).

These results confirm that statins could be used to inhibit SMC-induced restenosis, since they inhibit SMC proliferation and migration, as corroborated by literature data as well [24,28,29].

Moreover, CA-NP are suitable for delivering, in an effective and rapid manner, a drug to cells, maintaining its pharmacological properties and therapeutic effects. Some examples of statin loaded NP are described in the literature. Pitavastatin-containing nanoparticle were incorporated into eluting stent and reduced in-stent restenosis in an animal model [25] or intravenously infused thus inhibiting left ventricular remodeling [40] or atherosclerotic plaque destabilization [41]. However, the intravenous injection of nanoparticles systemically delivers the drug to inflammatory cells (mainly monocytes) [40], thus reducing the chance to reach other targets, such as SMC and endothelial cells.

CONCLUSION

Percutaneous transluminal angioplasty, which allows the disruption of the atheroma, is the main solution to open the narrowed, or obstructed artery. The main adverse event connected to this

procedure is the restenosis, an inflammatory process leading to the re-occlusion of the vessel. Among different techniques proposed to address this issue, the main solution resides in stenting the vessel or, if it is no possible, in administering locally a drug by an eluting balloon. This approach would take advantage prolonging the drug residence time in the injured artery by administering drug eluting nanoparticles. Indeed, the efficacy could rely on both the drug released into cells after nanoparticles uptake and the drug passively released in the extra-cellular matrix. Furthermore, SMC represent a promising pharmacological target since and their migration should be preferentially blocked to avoid the neointima formation; at the same time endothelial cells should be preserved since their migration favor the safety of the vessel. This work presents a proof-of- concept of FLV-NP which present the potentiality to inhibit the SMC migration, without altering the FLV effect on proliferation and migration of endothelial cells at the same nanoparticle concentration. Data on in vitro experiments showed that the endothelial cell vitality was significantly reduced when treated with a 1 μM FLV solution, while that of SMC was unaffected. Conversely, when the two cell lines were treated with FLV-NP, SMC appeared more sensible to FLV treatment than endothelial cells since SMC proliferation was significantly inhibited at 4 μM, while the toxic effect in endothelial cells was observed only at a higher concentration (10 μM).

In conclusion, the improved trophism on nanoparticles towards SMC combined with the excellent biocompatibility and low modification of microenvironment pH upon polymer degradation makes g-CA-PLGA a good candidate for the design of drug eluting balloons.

AUTHOR INFORMATION

Corresponding Author

* Professor Francesco Cilurzo, PhD

Department of Pharmaceutical Sciences, Università degli Studi di Milano,

via G. Colombo, 71 – 20133 Milan, Italy

telephone: +39 02 503 24635

fax: +39 02 503 24657

email: francesco.cilurzo@unimi.it

Present Addresses

†Confindustria Dispositivi Medici, via Burigozzo, 1A, - 20122 Milan, Italy

Author Contributions

FC and VT conceptualized the work; SB, FS, FP, LR, FC and PP designed the experiments and interpreted the data. GM, ES, CR and PS conducted the experiments and contributed to the data analysis. All authors have drafted the work, read and approved the final manuscript.

Funding Sources

No funds.

REFERENCES

(1) Fleiner, M.; Kummer, M.; Mirlacher, M.; Sauter, G.; Cathomas, G.; Krapf, R.; Biedermann, B. C. Arterial Neovascularization and Inflammation in Vulnerable Patients. *Circulation* **2004**, *110* (18), 2843–2850. https://doi.org/10.1161/01.cir.0000146787.16297.e8.

(2) Cassese, S.; Byrne, R. A.; Tada, T.; Pinieck, S.; Joner, M.; Ibrahim, T.; King, L. A.; Fusaro, M.; Laugwitz, K.-L.; Kastrati, A. Incidence and Predictors of Restenosis after Coronary Stenting in 10 004 Patients with Surveillance Angiography. *Heart* **2014**, *100* (2), 153–159. https://doi.org/10.1136/heartjnl-2013-304933.

(3) Prasad, K. Do Statins Have a Role in Reduction/Prevention of Post-PCI Restenosis? *Cardiovasc. Ther.* **2013**, *31* (1), 12–26. https://doi.org/10.1111/j.1755-5922.2011.00302.x.

(4) Kastrati, A.; Schömig, A.; Dietz, R.; Neumann, F. J.; Richardt, G. Time Course of Restenosis during the First Year after Emergency Coronary Stenting. *Circulation* **1993**, *87* (5), 1498–1505.

(5) Kim, M. S.; Dean, L. S. In-Stent Restenosis. *Cardiovasc. Ther.* **2011**, *29* (3), 190–198. https://doi.org/10.1111/j.1755-5922.2010.00155.x.

(6) Waksman, R.; Pakala, R. Drug-Eluting Balloon: The Comeback Kid? *Circ. Cardiovasc. Interv.* **2009**, *2* (4), 352–358. https://doi.org/10.1161/CIRCINTERVENTIONS.109.873703.

(7) Bukka, M.; Rednam, P. J.; Sinha, M. Drug-Eluting Balloon: Design, Technology and Clinical Aspects. *Biomed. Mater.* **2018**, *13* (3), 032001. https://doi.org/10.1088/1748-605X/aaa0aa.

(8) Spaulding, C. Drug-Eluting Balloons Are Coming, But Are We Ready? *Cardiovasc. Revascularization Med.* **2022**, *35*, 83–84. https://doi.org/10.1016/j.carrev.2021.11.020.

(9) Iyer, R.; Kuriakose, A. E.; Yaman, S.; Su, L.-C.; Shan, D.; Yang, J.; Liao, J.; Tang, L.; Banerjee, S.; Xu, H.; et al. Nanoparticle Eluting-Angioplasty Balloons to Treat Cardiovascular Diseases. *Int. J. Pharm.* **2019**, *554*, 212–223. https://doi.org/10.1016/J.IJPHARM.2018.11.011.

(10) Shah, P.; Chandra, S. Review on Emergence of Nanomaterial Coatings in Bio-Engineered Cardiovascular Stents. *J. Drug Deliv. Sci. Technol.* **2022**, *70*, 103224. https://doi.org/10.1016/j.jddst.2022.103224.

(11) Chen, J.; Zhang, X.; Millican, R.; Sherwood, J.; Martin, S.; Jo, H.; Yoon, Y.; Brott, B. C.; Jun, H.-W. Recent Advances in Nanomaterials for Therapy and Diagnosis for Atherosclerosis. *Adv. Drug Deliv. Rev.* **2021**, *170*, 142–199. https://doi.org/10.1016/j.addr.2021.01.005.

(12) Ko, K. W.; Choi, B.; Kang, E. Y.; Shin, S. W.; Baek, S. W.; Han, D. K. The Antagonistic Effect of Magnesium Hydroxide Particles on Vascular Endothelial Activation Induced by Acidic PLGA Degradation Products. *Biomater. Sci.* **2021**, *9* (3), 892–907. https://doi.org/10.1039/d0bm01656j.

(13) Anderson, J. M.; Shive, M. S. Biodegradation and Biocompatibility of PLA and PLGA Microspheres. *Adv. Drug Deliv. Rev.* **2012**, *64* (SUPPL.), 72–82. https://doi.org/10.1016/j.addr.2012.09.004.

(14) de Prado, A. P.; Perez-Martinez, C.; Cuellas, C.; Gonzalo-Orden, J. M.; Diego, A.; Regueiro, M.; Martinez-Fernandez, B.; Altonaga, J. R.; Marin Francisco, J. G.; Fernandez-Vazquez, F. Preclinical Evaluation of Coronary Stents: Focus on Safety Issues. *Curr. Vasc. Pharmacol.* **2013**, *11* (1), 74–99.

(15) Stowell, C. E. T.; Wang, Y. Quickening: Translational Design of Resorbable Synthetic Vascular Grafts. *Biomaterials* **2018**, *173*, 71–86. https://doi.org/10.1016/j.biomaterials.2018.05.006.

(16) Cilurzo, F.; Puoci, F.; Selmin, F.; Iemma, F.; Minghetti, P. Pyrogallic Acid-PLGA Conjugate as New Biodegradable Material Suitable for Final Sterilization by Irradiation. *Polym. Adv. Technol.* **2011**, *22* (12), 2201–2205. https://doi.org/10.1002/pat.1746.

(17) Selmin, F.; Puoci, F.; Parisi, O.; Franzé, S.; Musazzi, U.; Cilurzo, F. Caffeic Acid-PLGA Conjugate to Design Protein Drug Delivery Systems Stable to Irradiation. *J. Funct. Biomater.* **2015**, *6* (1), 1–13. https://doi.org/10.3390/jfb6010001.

(18) Katsanos, K.; Spiliopoulos, S.; Kitrou, P.; Krokidis, M.; Karnabatidis, D. Risk of Death Following Application of Paclitaxel-Coated Balloons and Stents in the Femoropopliteal Artery of the Leg: A Systematic Review and Meta-Analysis of Randomized Controlled Trials. *J. Am. Heart Assoc.* **2018**, *7* (24). https://doi.org/10.1161/JAHA.118.011245.

(19) Minghetti, P.; Cilurzo, F.; Selmin, F.; Casiraghi, A.; Grignani, A.; Montanari, L. Sculptured Drug-Eluting Stent for the on-Site Delivery of Tacrolimus. *Eur. J. Pharm. Biopharm.* **2009**,

73 (3). https://doi.org/10.1016/j.ejpb.2009.08.004.

(20) Iglesias, J. F.; Muller, O.; Heg, D.; Roffi, M.; Kurz, D. J.; Moarof, I.; Weilenmann, D.; Kaiser, C.; Tapponnier, M.; Stortecky, S.; et al. Biodegradable Polymer Sirolimus-Eluting Stents versus Durable Polymer Everolimus-Eluting Stents in Patients with ST-Segment Elevation Myocardial Infarction (BIOSTEMI): A Single-Blind, Prospective, Randomised Superiority Trial. *Lancet* **2019**, *394* (10205), 1243–1253. https://doi.org/10.1016/S0140-6736(19)31877-X.

(21) Stone, G. W.; Sabik, J. F.; Serruys, P. W.; Simonton, C. A.; Généreux, P.; Puskas, J.; Kandzari, D. E.; Morice, M.-C.; Lembo, N.; Brown, W. M.; et al. Everolimus-Eluting Stents or Bypass Surgery for Left Main Coronary Artery Disease. *N. Engl. J. Med.* **2016**, *375* (23), 2223–2235. https://doi.org/10.1056/NEJMoa1610227.

(22) Bellosta, S.; Ferri, N.; Arnaboldi, L.; Bernini, F.; Paoletti, R.; Corsini, A. Pleiotropic Effects of Statins in Atherosclerosis and Diabetes. *Diabetes Care* **2000**, *23* (SUPPL. 2).

(23) Comparato, C.; Altana, C.; Bellosta, S.; Baetta, R.; Paoletti, R.; Corsini, A. Clinically Relevant Pleiotropic Effects of Statins: Drug Properties or Effects of Profound Cholesterol

Reduction? *Nutr. Metab. Cardiovasc. Dis.* **2001**, *11* (5).

(24) Takemoto, M.; Liao, J. K. Pleiotropic Effects of 3-Hydroxy-3-Methylglutaryl Coenzyme a Reductase Inhibitors. *Arterioscler. Thromb. Vasc. Biol.* **2001**, *21* (11), 1712–1719.

(25) Tsukie, N.; Nakano, K.; Matoba, T.; Masuda, S.; Iwata, E.; Miyagawa, M.; Zhao, G.; Meng, W.; Kishimoto, J.; Sunagawa, K.; et al. Pitavastatin-Incorporated Nanoparticle-Eluting Stents Attenuate In-Stent Stenosis without Delayed Endothelial Healing Effects in a Porcine Coronary Artery Model. *J. Atheroscler. Thromb.* **2013**, *20* (1), 32–45. https://doi.org/10.5551/jat.13862.

(26) Corsini, A.; Bellosta, S.; Baetta, R.; Fumagalli, R.; Paoletti, R.; Bernini, F. New Insights into the Pharmacodynamic and Pharmacokinetic Properties of Statins. *Pharmacol Ther* **1999**, *84* (3), 413–428. https://doi.org/10.1016/S0163-7258(99)00045-5.

(27) Bellosta, S.; Bernini, F.; Ferri, N.; Quarato, P.; Canavesi, M.; Arnaboldi, L.; Fumagalli, R.; Paoletti, R.; Corsini, A. Direct Vascular Effects of HMG-CoA Reductase Inhibitors. *Atherosclerosis* **1998**, *137* (SUPPL.). https://doi.org/10.1016/S0021-9150(97)00319-5.

(28) Bellosta, S.; Arnaboldi, L.; Gerosa, L.; Canavesi, M.; Parente, R.; Baetta, R.; Paoletti, R.;

Corsini, A. Statins Effect on Smooth Muscle Cell Proliferation. *Semin. Vasc. Med.* **2004**, *4* (4). https://doi.org/10.1055/s-2004-869591.

(29) Corsini, A.; Bellosta, S.; Baetta, R.; Fumagalli, R.; Paoletti, R.; Bernini, F. New Insights into the Pharmacodynamic and Pharmacokinetic Properties of Statins. *Pharmacol. Ther.* **1999**, *84* (3), 413–428. https://doi.org/10.1016/S0163-7258(99)00045-5.

(30) Bellosta, S.; Via, D.; Canavesi, M.; Pfister, P.; Fumagalli, R.; Paoletti, R.; Bernini, F. HMG-CoA Reductase Inhibitors Reduce MMP-9 Secretion by Macrophages. *Arterioscler. Thromb. Vasc. Biol.* **1998**, *18* (11), 1671–1678. https://doi.org/10.1161/01.ATV.18.11.1671.

(31) Desai, P.; Helkin, A.; Odugbesi, A.; Stein, J.; Bruch, D.; Lawler, J.; Maier, K. G.; Gahtan, V. Fluvastatin Inhibits Intimal Hyperplasia in Wild-Type but Not Thbs1-Null Mice. *J. Surg. Res.* **2017**, *210*, 1–7. https://doi.org/10.1016/j.jss.2016.10.007.

(32) Laquintana, V.; Denora, N.; Musacchio, T.; Lasorsa, M.; Latrofa, A.; Trapani, G. Peripheral Benzodiazepine Receptor Ligand-PLGA Polymer Conjugates Potentially Useful as Delivery Systems of Apoptotic Agents. *J. Control. Release* **2009**, *137* (3), 185–195.

https://doi.org/10.1016/j.jconrel.2009.04.007.

(33) Huynh, K. A.; Chen, K. L. Aggregation Kinetics of Citrate and Polyvinylpyrrolidone Coated Silver Nanoparticles in Monovalent and Divalent Electrolyte Solutions. *Environ. Sci. Technol.* **2011**, *45* (13), 5564–5571. https://doi.org/10.1021/es200157h.

(34) Liu, J.; Pu, H.; Chen, C.; Liu, Y.; Bai, R.; Kan, J.; Jin, C. Reaction Mechanisms and Structural and Physicochemical Properties of Caffeic Acid Grafted Chitosan Synthesized in Ascorbic Acid and Hydroxyl Peroxide Redox System. *J. Agric. Food Chem.* **2018**, *66* (1), 279–289. https://doi.org/10.1021/acs.jafc.7b05135.

(35) Parisi, O. I.; Ruffo, M.; Malivindi, R.; Vattimo, A. F.; Pezzi, V.; Puoci, F. Molecularly Imprinted Polymers (MIPs) as Theranostic Systems for Sunitinib Controlled Release and Self-Monitoring in Cancer Therapy. *Pharmaceutics* **2020**, *12* (1). https://doi.org/10.3390/pharmaceutics12010041.

(36) Uyama, H.; Maruichi, N.; Tonami, H.; Kobayashi, S. Peroxidase-Catalyzed Oxidative Polymerization of Bisphenols. *Biomacromolecules* **2002**, *3* (1), 187–193. https://doi.org/10.1021/bm0101419.

(37) Cirillo, G.; Puoci, F.; Iemma, F.; Curcio, M.; Parisi, O. I.; Spizzirri, U. G.; Altimari, I.; Picci, N. Starch-Quercetin Conjugate by Radical Grafting: Synthesis and Biological Characterization. *Pharm. Dev. Technol.* **2012**, *17* (4), 466–476. https://doi.org/10.3109/10837450.2010.546413.

(38) Panyam, J.; Labhasetwar, V. Dynamics of Endocytosis and Exocytosis of Poly(D,L-Lactide-Co-Glycolide) Nanoparticles in Vascular Smooth Muscle Cells. *Pharm. Res.* **2003**, *20* (2), 212–220. https://doi.org/10.1023/A:1022219003551.

(39) Bellosta, S.; Ferri, N.; Bernini, F.; Paoletti, R.; Corsini, A. Non-Lipid-Related Effects of Statins. *Ann Med* **2000**, *32* (3), 164–176. https://doi.org/10.3109/07853890008998823.

(40) Mao, Y.; Koga, J.; Tokutome, M.; Matoba, T.; Ikeda, G.; Nakano, K.; Egashira, K. Nanoparticle-Mediated Delivery of Pitavastatin to Monocytes/Macrophages Inhibits Left Ventricular Remodeling After Acute Myocardial Infarction by Inhibiting Monocyte-Mediated Inflammation. *Int. Heart J.* **2017**, *58* (4), 615–623. https://doi.org/10.1536/ihj.16-457.

(41) Katsuki, S.; Matoba, T.; Nakashiro, S.; Sato, K.; Koga, J.; Nakano, K.; Nakano, Y.; Egusa,

S.; Sunagawa, K.; Egashira, K. Nanoparticle-Mediated Delivery of Pitavastatin Inhibits Atherosclerotic Plaque Destabilization/Rupture in Mice by Regulating the Recruitment of Inflammatory Monocytes. *Circulation* **2014**, *129* (8), 896–906. https://doi.org/10.1161/CIRCULATIONAHA.113.002870.